A Metamaterial Inspired Compact Miniaturized Triple-band Near Field Resonant Parasitic Antenna for WLAN/WiMAX Applications

Si Li [1], Atef Z. Elsherbeni [2], Zhenfeng Ding [3], and Yunlong Mao [1]

[1] School of Electronics and Information
Jiangsu University of Science and Technology, Zhenjiang, Jiangsu 212003, China
lisi0511@just.edu.cn, maoyunlong0511@just.edu.cn

[2] Electrical Engineering Department
Colorado School of Mines, CO 80401 USA
aelsherb@mines.edu

[3] Research Institute of Petroleum Exploration and Development
PetroChina Company Limited, Beijing 100083, China
815703534@qq.com

Abstract ─ This paper presents a metamaterial-inspired triple-band antenna specified for WLAN and WiMAX applications with a compact size of 24mm × 18mm × 1mm (at 2.4 GHz). It consists of a dual-band left-handed metamaterial (LHM) unit surrounded by a G-style monopole antenna. The LHM is first designed and analyzed with equivalent circuits and simulations. A loop antenna based on the LHM unit is designed and simulated to investigate the radiating performance of the LHM unit structure. We also ran simulations for the G-style monopole. Later, the LHM unit is employed as a near-field resonant parasitic (NFRP) element that surrounded by the G-style monopole. A prototype of this antenna is fabricated. Simulations and measurements were carried out and the results match well, identifying good omni-directional radiating performance. Radiation comparisons with the loop antenna and the G-style monopole indicate that due to NFRP, the G-style monopole's pass bands are shifted to lower frequencies to satisfy 2.45 GHz and 5.5 GHz bands requirements, meanwhile the LHM unit structure operates a third pass band of 3.5 GHz. The compact size and good radiation properties of the antenna render it suitable for WLAN/ WiMAX applications.

Index Terms ─ Left-handed metamaterial, miniaturized antenna, WLAN/WiMAX.

I. INTRODUCTION

With the rapid development of wireless communications, the demand for antennas with compact size and multiband property has greatly increased. A lot of investigations were conducted to satisfy the wireless local area network (WLAN) standard of 2.4 GHz to 2.484 GHz / 5.15 GHz to 5.35 GHz / 5.75 GHz to 5.825 GHz, and the World Wide Interoperability for Microwave Access (WiMAX) standard of 3.4 GHz to 3.69 GHz / 5.25 GHz to 5.85 GHz requirements. Various types of miniaturized WLAN / WiMAX antennas have been reported, among which printed monopole antennas have been widely used because of their low cost, light weight and good performance. Such that in [1], F shaped slots were etched on the rectangular radiating patch and a circular disc printed on the other side of the substrate, achieving wide band coverage and good radiating performance; in [2], a high gain dual-band slot antenna was presented based on an ultra wide band slot radiating element.

Recently, metamaterials (MTMs) have arouse great attentions due to their unique properties in antenna designs [3]. Efforts to miniaturize and compactify antennas have employed composite right/left handed transmission lines (CRLH-TLs) and multiple electrically small near-field resonant parasitic (NFRP) elements. However, even though CRLH-TL may brought higher level miniaturization since its zeroth resonance is independent with size, high quality factors make the corresponding operating bands extremely narrow [4-8]. Comparably, NFRP elements can be designed and adjusted independently, thereby offering additional degree of freedom in antenna designs [9, 10]. The operating principle of NFRP is illustrated in Fig. 1. In general, NFRP elements can be divided into 2 categories, i.e., electric-driven and magnetic-driven NFRP [11], depending on how they coupled to antennas. Meander lines [11] and split ring resonators (SRR) [12] are representative NFRP elements reported and significant miniaturization were achieved [13, 14]. Besides, good

Submitted On: July 2, 2020
Accepted On: November 30, 2020
https://doi.org/10.47037/2020.ACES.J.351213

radiating performance can also be obtained with improved impedance matching due to NFRP coupling [15].

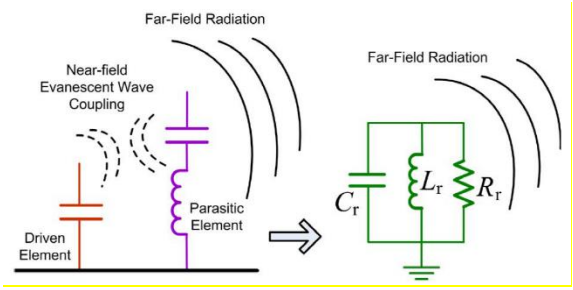

Fig. 1. Illustration of NFRP.

In this paper, a metamaterial-inspired compact miniaturized triple-band NFRP antenna for WLAN/ WiMAX applications is presented. A dual-band left-handed metamaterial (LHM) is first designed and analyzed with equivalent circuits and full-wave simulations. Then this LHM unit is employed as NFRP element that surrounded by a G-style monopole antenna. We investigated the radiating performance of the G-style monopole, a loop antenna based on the designed LHM unit and the final proposed NFRP antenna, figured out that the near-field resonate coupling makes the working bands of the G-style monopole shift to lower frequencies to meet 2.4GHz and 5.5 GHz WLAN/WiMAX requirements, while the LHM unit itself operates additional frequency band from 3.40 GHz to 3.69 GHz. A prototype of the proposed antenna is fabricated and measured, the results match well to the simulated ones, indicating good omni-directional radiating performance at WLAN / WiMAX frequency ranges.

II. LHM DESIGN AND ANALYSIS

A. LHM design

A novel LHM unit is designed, as illustrated in Fig. 2, where metallic strips are printed on a 1 mm-thick FR4 whose relative permittivity is 4.4. Optimized parameters are a = 10 mm, b = 8.3 mm, c = 0.5 mm, w = 1 mm, and the gap g = 0.2mm.

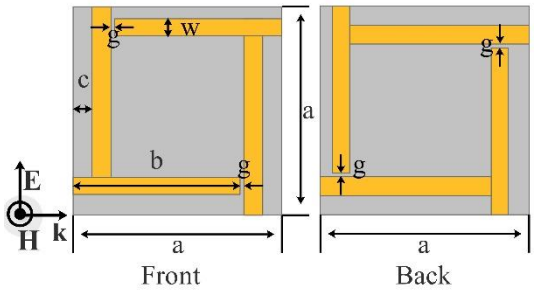

Fig. 2. Structure of the designed LHM unit.

B. Equivalent circuit analysis

The designed LHM is at least capable of generating two magnetic resonances and two electric resonances from its metallic structure [16]. The first magnetic resonance comes from the rectangular loop of the metallic structure. Its equivalent circuit is illustrated in Fig. 3, where L_1 is the self-inductance of each strip, C_g is the gap capacitance, and C_s is the surface capacitance.

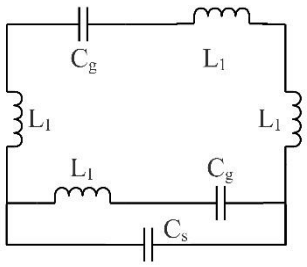

Fig. 3. Equivalent circuit of the first magnetic resonance.

According to the strip line theory [17], the inductance of a strip line can be calculated using:

$$L = 2\times10^{-4} l\left[ln\left(\frac{l}{w+t}\right)+1.193+0.2235\frac{w+t}{l}\right]. \quad (1)$$

Where *l* is the length, *w* is the width, and *t* is the thickness of the strip line. For convenience, we define a function to represent the calculation of the inductance of (1) as *Cal_induc(w, l, t)*.

The capacitance per unit length of the paralleled strip lines, C_{pul}, is calculated using:

$$C_{pul} = \varepsilon_0 \varepsilon_e F(k). \quad (2)$$

Where ε_0 is the permittivity of free space, ε_e and *F(k)* are given as:

$$\varepsilon_e = 1+(\varepsilon_r - 1)F(k)/2F(k1), \quad (3)$$

$$F(k) = \begin{cases} \frac{1}{\pi}\ln(2\frac{1+\sqrt{k'}}{1-\sqrt{k'}}), & 0 < k \le \frac{1}{\sqrt{2}} \\ \pi\ln(2\frac{1+\sqrt{k}}{1-\sqrt{k}})^{-1}, & \frac{1}{\sqrt{2}} < k \le 1 \end{cases} \quad (4)$$

where

$$\begin{cases} a_e = g/2, b_e = a_e + w, \\ k = a_e / b_e \\ k1 = \dfrac{\sinh(\pi a_e / 2h)}{\sinh(\pi b_e / 2h)}, \\ k' = \sqrt{1-k^2} \end{cases} \quad (5)$$

and *g* is the gap width between two strips, *w* is the width of each strip, h is the thickness of the substrate, and ε_r is the relative permittivity. For convenience, we define a function $Cal\_cap(w, g, h, \varepsilon_r)$ to represent capacitance of (2).

For the case when the strips are on different sides of the substrate, the capacitance can be calculated using:

$$C = \frac{\varepsilon_r \varepsilon_0 S}{d}, \tag{6}$$

where S is the paralleled area, d is the distance between the strips.

When the gap capacitance C_g is too small, the surface capacitance should be taken into consideration. The calculation for surface capacitance is simplified as the summation of the paralleled strips together.

Accordingly, we obtain:

$$\begin{cases} L_1 = Cal\_induc(w,b,t) \approx 5.51nH \\ C_g = w \times Cal\_cap(w, a-b-c-w, h, \varepsilon_r) \approx 0.05\,pF \\ C_s = 2 \times (b-c-w) \times Cal\_cap(w, a-2(c+w), h, \varepsilon_r) \\ \quad \approx 0.2\,pF \end{cases}. \tag{7}$$

Therefore, the first magnetic resonant frequency is:

$$f_{m1} = \frac{1}{2\pi\sqrt{4L_1 \times \left(C_s + C_g/2\right)}} \approx 2.25GHz. \tag{8}$$

The second magnetic resonance mainly comes from the mutual coupling between the metallic structures on different sides of the substrate. Before the equivalent circuit analysis, the capacitance constitution under this situation should be introduced.

Figure 4 displayed the capacitance constitution. Unlike the single sided cases, both plane-parallel coupling and surface coupling contributes to the calculations of equivalent capacitance. It should also be noticed that the equivalent surface capacitance and gap capacitance only include the coupling through the air.

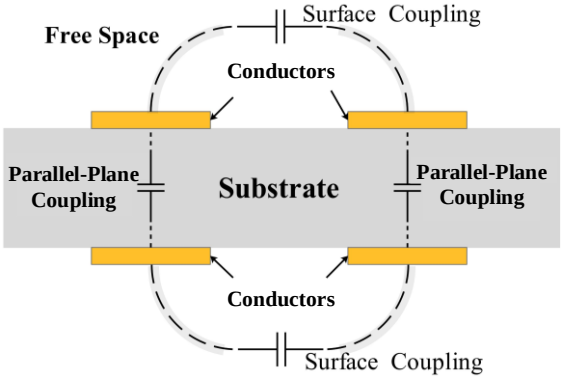

Fig. 4. Capacitance constitution illustration.

Since the proposed structure in Fig. 2 is symmetrical, it can be divided into 4 identical parts, of whom each part is composed of two paralleled metallic strips separated by the substrate. Hence, we built the equivalent circuit for each part first, and then connect them together as shown in Fig. 5. The surface capacitance are also equally distributed to each branch. Therefore, the equivalent circuit for the second magnetic resonance are obtained as illustrated in Fig. 5, where C_1 refers to the plane-parallel capacitor of the two paralleled strips on different sides of the substrate, C'_g and C'_s refer to the gap and surface capacitors, respectively.

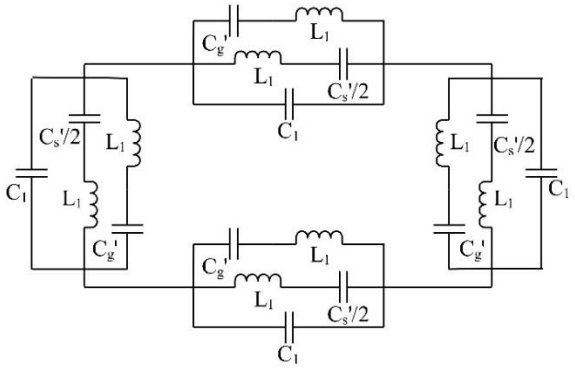

Fig. 5. Equivalent circuit for the second magnetic resonance.

According to the previous setup, we can obtain that:

$$\begin{cases} C_g' = \frac{1}{2} \times w \times Cal\_cap(w, a-b-c-w, h, \varepsilon_r = 1) \\ \quad \approx 0.01\,pF \\ C_s' = \frac{1}{2} \times 2(b-c-w) \times Cal\_cap(w, a-2(w+c)h, \varepsilon_r = 1) \\ \quad \approx 0.05\,pF \\ C_1 = \frac{\varepsilon_0 \varepsilon_r bw}{h} \approx 0.32\,pF. \end{cases} \tag{9}$$

Therefore, the second magnetic resonant frequency is:

$$f_{m2} = \frac{1}{2\pi\sqrt{2L_1 \times \left(C_1 + C'_g + C'_s/2\right)/4}} \approx 5.05GHz. \tag{10}$$

The analysis for the electric resonators is quite different. Vertically polarized electric field will activate vertical currents on the strips as illustrated in Fig. 6. For the first electric resonance whose equivalent circuit is also displayed in Fig. 6.

In this figure, C_2 refer to capacitance of two vertical neighboring strips of the upper and lower units, which is approximated as:

$$C_2 = (a-2c) \times Cal\_cap(w, 2c, h, \varepsilon_r) \approx 0.29\,pF. \tag{11}$$

Therefore, the first electric resonant frequency is:

$$f_{e1} = \frac{1}{2\pi\sqrt{3L_1 \times C_2}} \approx 2.30GHz. \tag{12}$$

Similarly, the equivalent circuit for the second electric resonator of a double sided units as illustrated in Fig. 7.

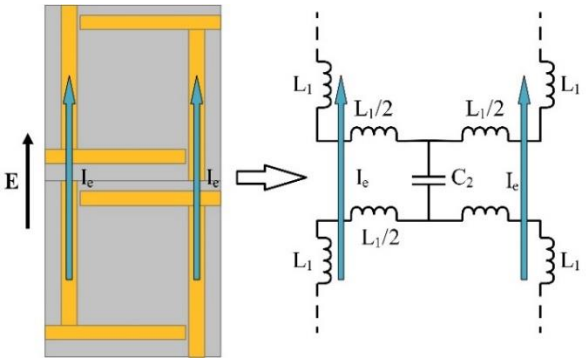

Fig. 6. Two LHM vertically position units and their equivalent circuit of the first electric resonator.

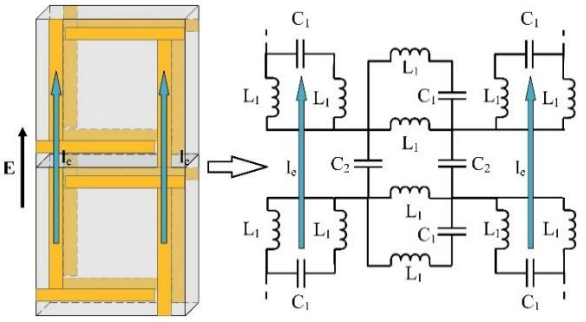

Fig. 7. Equivalent circuit of the second electric resonator.

Hence it is concluded that the equivalent inductance L_e and the equivalent capacitance C_e should be:

$$\begin{cases} L_e = L_1 \\ C_e = 2C_1 \,||\, C_2 \approx 0.2\,pF \end{cases}. \tag{13}$$

Therefore, the second electric resonant frequency is obtained:

$$f_{e2} = \frac{1}{2\pi\sqrt{L_e \times C_e}} \approx 4.80GHz. \tag{14}$$

C. Simulation and analysis

Simulations were operated using HFSS to get the S parameters. The magnitude of S_{11} and S_{21} are displayed in Fig. 8. Due to the high loss of the substrate, passing band property of this LHM is not very good.

The effective permeability and permittivity are retrieved with the help of 'S parameter retrieval' method in [18]. Figure 9 displayed the real part of effective permeability μ_{eff}, permittivity ε_{eff} and refractive index n of the LHM. It is observed that double negative properties are from 2.12 to 2.45 GHz, 4.84 to 5.08 GHz, and 5.19 to 5.42 GHz, respectively. The first and second negative bands match well with our analysis. The third one needs further investigation and will not be discussed here. These LHM bands are very close to the WLAN/ WiMAX bands.

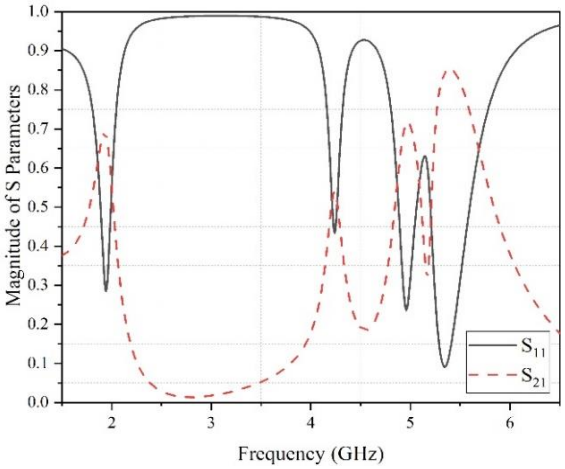

Fig. 8. Magnitude of simulated S parameters of the proposed LHM.

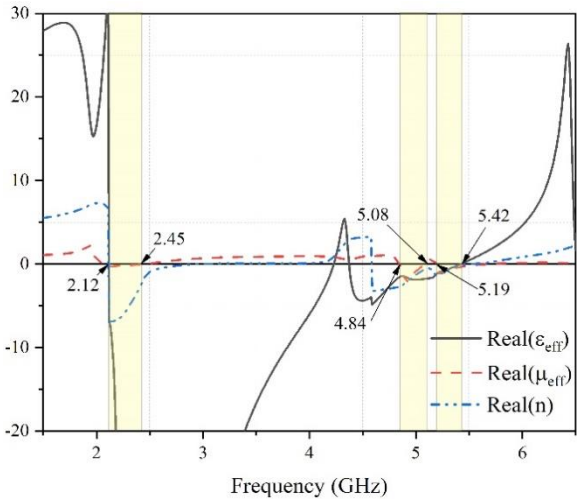

Fig. 9. Retrieved effective parameters of the proposed LHM.

III. LHM INSPIRED ANTENNA: DESIGN AND ANALYSIS

A. Analysis of a loop antenna using the LHM unit

Since we want to use the LHM unit not only for NFRP, but also as a loop antenna, it is essential to discuss the radiating property of this LHM unit with proper feed to serve as a loop antenna. The structure is displayed in Fig. 10. Parameters are L_s = 24mm, W_s = 18mm, L_g = 8.5mm, L_f = 11mm, W_f = 3mm, W_2=6mm, and W_g =7.2mm. This antenna is printed on a FR4 substrate with a thickness of 1mm.

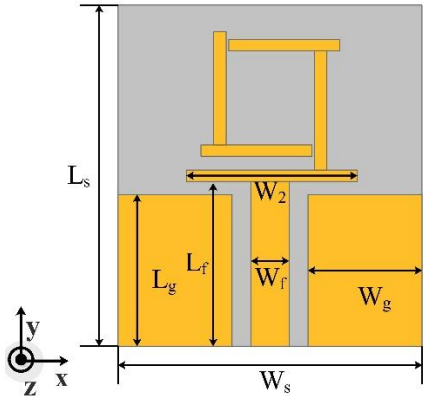

(a) Front view

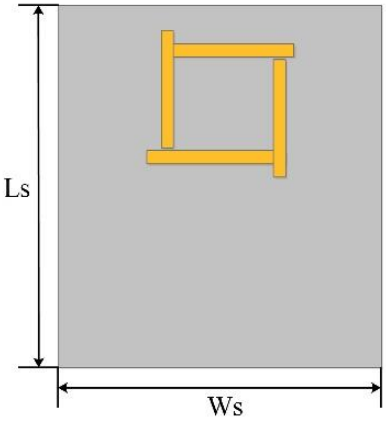

(b) Back view

Fig. 10. Structure of the proposed antenna: (a) front view and (b) back view.

The simulated S_{11} is displayed in Fig. 11. There are two pass bands as observed, of which one is from 2.49 GHz to 2.58 GHz, and the other one is from 3.71 GHz to 4.34 GHz. The 2 resonant frequencies are 2.54 GHz and 4 GHz, respectively.

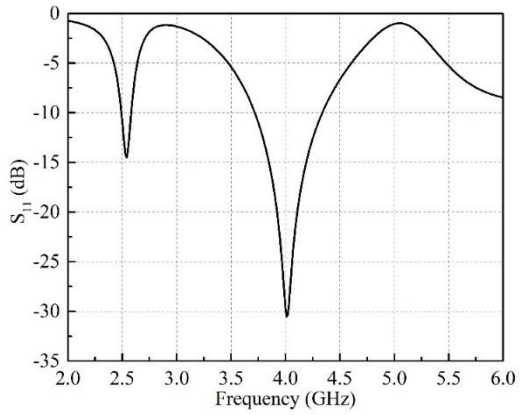

Fig. 11. Simulated S parameter of the LHM antenna.

B. Analysis of G-style monopole antenna

A G-style monopole antenna is designed as displayed in Fig. 12 with parameters listed in Table 1.

Table 1: Parameters for G-style monopole (Unit: mm)

Parameters	L_1	L_2	L_3	L_f	L_g	L_s
Length	4.7	12.4	7	11	8.5	24
Parameters	W_1	W_2	W_3	W_f	W_g	W_s
Length	1	10.4	2	3	7.2	18

This antenna is a normal dual-band monopole. It is obvious that the lengths of the two branches decide its operating bands. We ran simulations for this antenna, and the results are shown in Fig. 13. It is observed that the first passing band is ranging from 2.76 GHz to 3.03 GHz, while the second passing band is ranging from 5.2 GHz to 7.68 GHz.

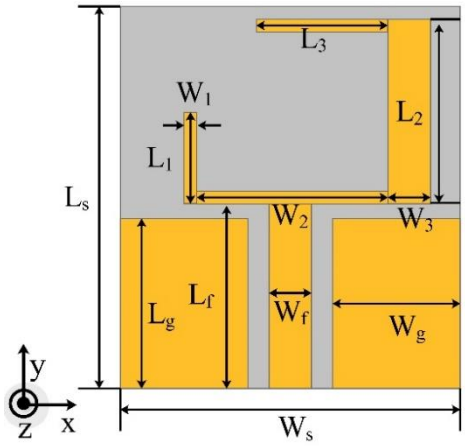

Fig. 12. Structure of the G-style monopole antenna.

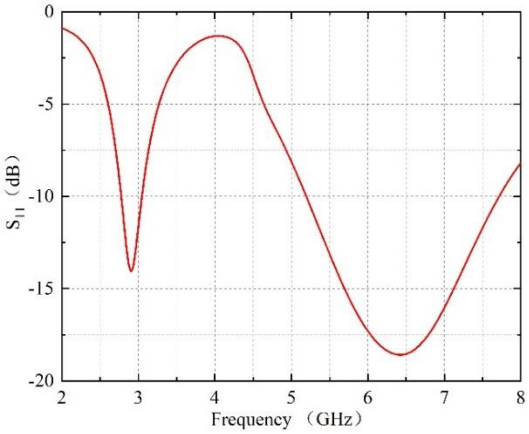

Fig. 13. Simulated S_{11} of the G-style antenna.

C. LHM inspired antenna

The G-style monopole antenna is then used to surround the designed LHM unit, as illustrated in Fig.

14. The lengths of the parameters are exactly the same as listed previously in Table 1. The gap between the LHM unit and the G-style monopole g_1 = 0.5mm.

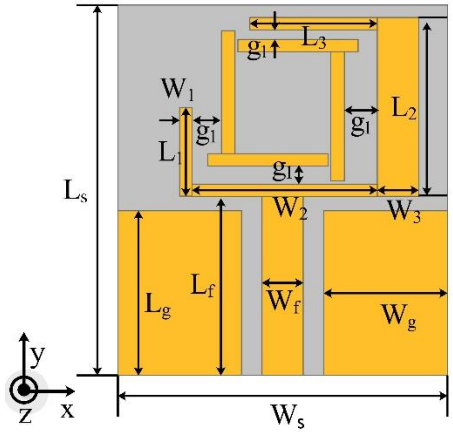

(a) Front view

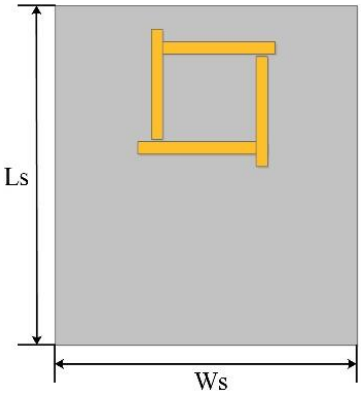

(b) Back view

Fig. 14. Structure of the LHM inspired antenna.

We ran simulations with HFSS and CST for the LHM inspired antenna, respectively. Furthermore, a prototype of the antenna is fabricated and its radiating performance are measured in a microwave chamber as displayed in Fig. 15.

The simulated and measured S_{11} for the LHM inspired antenna are displayed in Fig. 16. It is observed that there are 3 pass bands, of whom the first one is from 2.4 GHz to 2.52 GHz, the second one is from 3.4 GHz to 3.69 GHz, and the third one is from 4.47 GHz to 6 GHz, covering the requirements of WLAN and WiMAX. The measured S_{11} matches well with the simulated one.

The peak gain and efficiency of the LHM inspired antenna at different frequencies are displayed in Fig. 17. It is observed that at the frequencies of 2.4 GHz to 2.5 GHz, the simulated peak gain is ranging from 0.73 dBi to 1.11 dBi, and the efficiency is ranging from 71.5% to 81.3%; at 3.4 GHz to 3.69 GHz, the peak gain is ranging from 1.25 dBi to 1.54 dBi, and the efficiency is ranging from 78.2% to 88.5%; at 5.15 GHz to 5.85 GHz, the peak gain is ranging from 2.45 dBi to 3 dBi, and the efficiency is ranging from 93.9% to 95.4%.

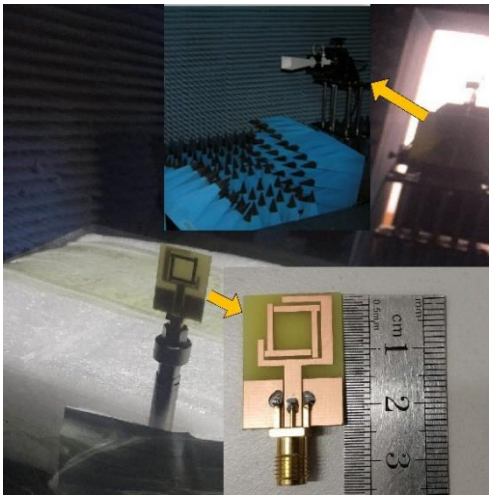

Fig. 15. A Fabricated prototype and measurement facilities.

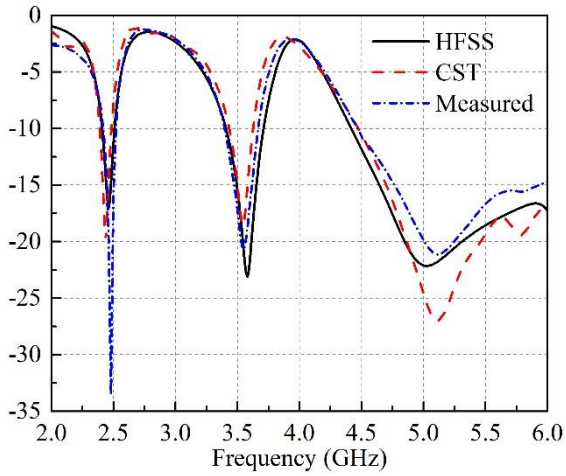

Fig. 16. Simulated and measured S_{11} of the LHM inspired antenna.

Radiation patterns of the proposed antenna are also simulated and measured. Due to the facility limitation, only normalized pattern is measured. Figures 18 (a) to (f) displayed the simulated (dashed lines) and measured (solid lines) normalized radiation pattern of the LHM inspired antenna on YOZ plane (black) and XOZ plane (red) at 2.45 GHz, 3.5 GHz, 3.6 GHz, 5.2 GHz, 5.5 GHz, and 5.8 GHz, respectively. As observed, the proposed antenna exhibits good omni-directional performance at all the discussed frequencies.

Therefore, the gain, efficiency and radiation patterns of the LHM inspired antenna indicate that this antenna exhibits good radiation performance for WLAN/WiMAX applications.

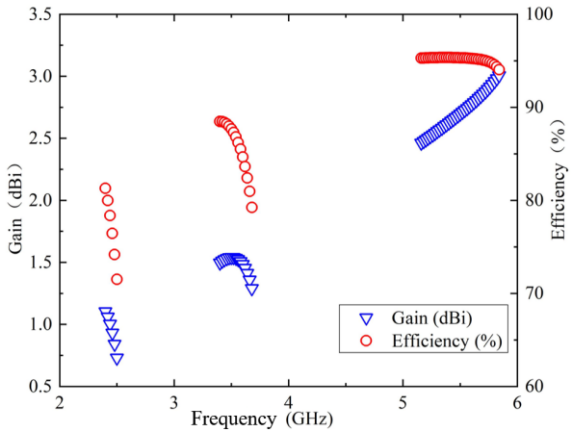

Fig. 17. Simulated gain and efficiency at frequency ranges of 2.4 to 2.5 GHz, 3.4 to 3.69 GHz, 5.15 to 5.85 GHz.

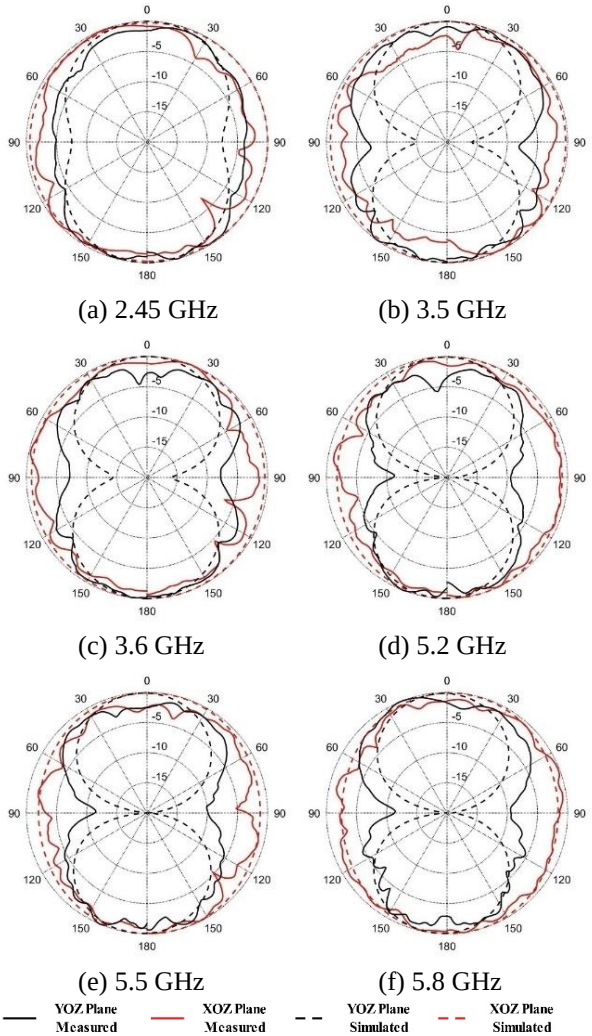

Fig. 18. Simulated (dashed lines) and Measured (solid lines) normalized radiation patterns of the LHM loaded antenna at: (a) 2.45 GHz, (b) 3.5 GHz, (c) 3.6 GHz, (d) 5.2 GHz, (e) 5.5 GHz, and (f) 5.8 GHz.

D. Discussions of electric current distributions

To further investigate the radiating property, surface current distributions of this LHM inspired NFRP antenna at 2.45 GHz, 3.5 GHz and 5.5 GHz are displayed in Figs. 19 (a) to (c), respectively.

At 2.45 GHz, the longer arm of the G-style structure is the main radiating element. Remarkable induced current is observed around the LHM unit structure. Therefore, near-field resonant coupling between the LHM unit and the G-style monopole played an important role to make the resonant frequencies shift to meet 2.45 GHz band requirement.

At 3.5 GHz, Strongest current is observed flowing around the LHM unit, identifying that the LHM unit is now turned to a loop radiator that fed through the coupling with the G-style structure.

At 5.5 GHz, the shorter arm of the G-style structure becomes the main radiator. Induced current is also observed flowing around the LHM unit, identifying that for this case, near-field resonant coupling will still serve as a parasitic element, shifting the resonant frequencies to meet the 5.5 GHz band requirement.

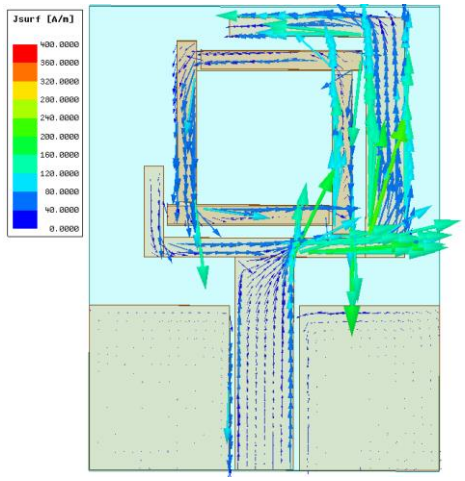

(a) 2.45 GHz

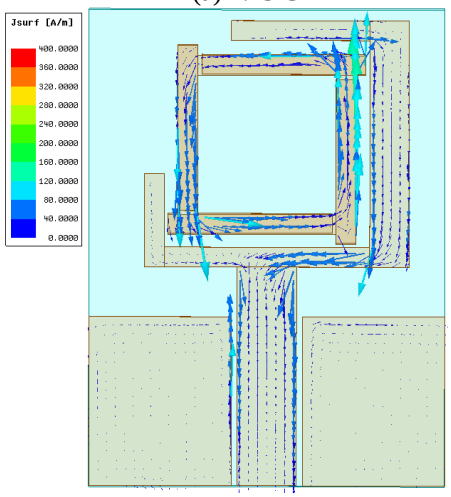

(b) 3.5 GHz

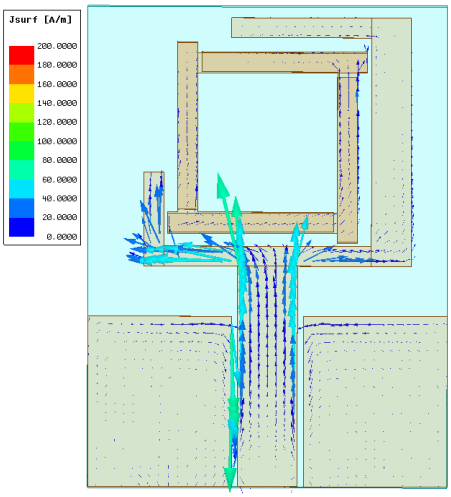

(c) 5.5 GHz

Fig. 19. Surface current distribution of the LHM inspired antenna at: (a) 2.45 GHz, (b) 3.5 GHz, and (d) 5.5 GHz.

Table 2 listed the comparisons of size and frequency coverage of the proposed antenna with some recently reported WLAN/WiMAX antennas.

Table 2: Comparison of sizes and operating frequency ranges with the proposed antenna

Ref. (year)	Size (mm^2)	Frequencies (GHz)		
		WLAN 2.4-2.484	WiMAX 3.4-3.69	WLAN & WiMAX 5.15-5.85
[1] (2016)	19×25	2.00-2.76	3.04-4.00	5.20-6.00
[19] (2016)	34×30	1.92-2.17	3.40-3.60	5.15-5.35
[20] (2016)	40×40	2.20-2.80	Not cover	5.20-7.00
[21] (2016)	28×32	2.29-2.88	3.26-3.88	4.17-6.07
[22] (2016)	24×22.5	2.39-2.52	3.34-3.67	4.43-5.97
[23] (2017)	26×29.4	2.23-2.89	3.21-4.45	5.32-5.85
[24] (2017)	22×45	2.12-3.06	Not cover	5.06-5.28
[6] (2018)	70×44	2.22-2.79	Not cover	5.42-6.04
[25] (2018)	23×17	0.48-6.5		
[26] (2019)	32×37.2	2.22-2.52	3.42-3.68	5.30-5.65
Proposed	24×18	2.40-2.52	3.40-3.69	4.47-6.00

From this table, it is drawn that the proposed antenna has a relatively small size while also provide a whole coverage of WLAN/WiMAX frequency ranges.

IV. CONCLUSION

This paper presents a metamaterial inspired miniaturized triple-band antenna with a compact size of $24 \times 18 \times 1$ mm^3 (at 2.4 GHz). A LHM is designed and analyzed with equivalent circuit and simulations. It is then employed as NFRP element that surrounded by a G-style monopole. To investigate the operating principle, we also ran simulations for the G-style monopole antenna, a loop antenna based on the LHM unit. The results indicate that the LHM unit made the operating bands correspond to the G-style monopole to lower frequencies, while the LHM unit itself is operating an additional passing band. A prototype of the proposed antenna is fabricated and measured. The results were in good agreement with the simulated ones, validating good radiating performance of the proposed metamaterial inspired antenna. Hence, the proposed antenna is a good candidate for WLAN/WiMAX applications.

ACKNOWLEDGMENT

This paper is supported by the Natural Science Foundation of Jiangsu province of China (BK20190956).

REFERENCES

[1] A. K. Gautam, L. Kumar, B. K. Kanaujia, and K. Rambabu, "Design of compact F-shaped slot triple-band antenna for WLAN/WiMAX applications," *IEEE Trans. Antennas Propag*., vol. 64, no. 3, pp. 1101-1105, 2016.

[2] M. V. Rooyen, J. W. Odendaal, and J. Joubert, "High-gain directional antenna for WLAN and WiMAX applications," *IEEE Antennas and Wireless Propagation Letters*, vol. 16, no. 99, pp. 286-289, 2017.

[3] A. D. Tadesse, O. P. Acharya, and S. Sahu, "Application of metamaterials for performance enhancement of planar antennas: A review," *International Journal of RF and Microwave Computer-Aided Engineering*, p. e22154, 2020. doi: 10.1002/mmce.22154.

[4] S. Yan and G. Vandenbosch, "Low-profile dual-band pattern diversity patch antenna based on composite right/left-handed transmission line," *IEEE Trans. Antennas Propag*., vol. PP, no. 99, pp. 1-1, 2017.

[5] C. Zhang, J. Gong, Y. Li, and Y. Wang, "Zeroth-order-mode circular microstrip antenna with patch-like radiation pattern," *IEEE Antennas and Wireless Propagation Letters*, vol. 17, no. 3, pp. 446-449, 2018.

[6] K. Sun, S. Han, J. Choi, and J. K. Lee, "Miniaturized active metamaterial resonant antenna with improved radiation performance based on negative-resistance-enhanced CRLH transmission lines," *IEEE Antennas and Wireless Propagation*

Letters, vol. 17, no. 7, pp. 1162-1165, 2018.

[7] G. Xiang, T. Jackson, and P. Gardner, "Multiband open-ended resonant antenna based on one ECRLH unit cell structure," *IEEE Antennas and Wireless Propagation Letters*, vol. 16, no. 99, pp. 1-1, 2017.

[8] Z. Wu, L. Li, X. Chen, and K. Li, "Dual-band antenna integrating with rectangular mushroom-like superstrate for WLAN applications," *IEEE Antennas & Wireless Propagation Letters*, vol. 15, pp. 1269-1272, 2016.

[9] A. Erentok and R. W. Ziolkowski, "Metamaterial-inspired efficient electrically small antennas," *IEEE Trans. Antennas Propag.*, vol. 56, no. 3, pp. 691-707, 2008.

[10] Y. Dong and T. Itoh, "Metamaterial-based antennas," *Proc. IEEE*, vol. 100, no. 7, pp. 2271-2285, 2012.

[11] T. Dong, X. Zhu, M. Li, Y. Zhang, B. Zhou, H. Zeng, and M.-C. Tang, "Design of electrically small Hilbert fractal NFRP magnetic monopole antennas," *Journal of Electromagnetic Waves and Applications*, vol. 33, no. 4, pp. 454-464, 2019.

[12] P. Pokkunuri, B. T. P. Madhav, and M. Venkateswararao, "Metamaterial inspired reconfigurable fractal monopole antenna for multi-band applications," *Int. J. Intell. Eng. Syst.*, vol. 12, pp. 53-61, 2019.

[13] M.-C. Tang, Y. Duan, Z. Wu, X. Chen, M. Li, and R. W. Ziolkowski, "Pattern reconfigurable, vertically polarized, low-profile, compact, near-field resonant parasitic antenna," *IEEE Trans. Antennas Propag.*, vol. 67, no. 3, pp. 1467-1475, 2018.

[14] K. E. Kedze, H. Wang, and I. Park, "Compact broadband omnidirectional radiation pattern printed dipole antenna incorporated with split-ring resonators," *IEEE Access*, vol. 6, pp. 49537-49545, 2018.

[15] M.-C. Tang, Y. Chen, and R. W. Ziolkowski, "Experimentally validated, planar, wideband, electrically small, monopole filtennas based on capacitively loaded loop resonators," *IEEE Trans. Antennas Propag.*, vol. 64, no. 8, pp. 3353-3360, 2016.

[16] S. Li, W. Yu, A. Z. Elsherbeni, W. Li, and Y. J. I. J. O. A. Mao, "A novel dual-band left-handed metamaterial design method," *International Journal of Antennas and Propagation*, vol. 2017, 2017.

[17] I. Bahl and P. Bhartia, *Microwave Solid State Circuit Design*. Wiley, 2003.

[18] X. Chen, T. M. Grzegorczyk, B. I. Wu, P. J. Jr, and J. A. Kong, "Robust method to retrieve the constitutive effective parameters of metamaterials," *Phys. Rev. E*, vol. 70, no. 1, pt. 2, pp. 811-811, 2004.

[19] A. R. Jalali, J. Ahamdi- Shokouh, and S. R. Emadian, "Compact multiband monopole antenna for UMTS, WiMAX, and WLAN applications," *Microwave & Optical Technology Letters*, vol. 58, no. 4, pp. 844-847, 2016.

[20] A. Pirooj, M. Naser-Moghadasi, and F. B. Zarrabi, "Design of compact slot antenna based on split ring resonator for 2.45/5 GHz WLAN applications with circular polarization," *Microwave & Optical Technology Letters*, vol. 58, no. 1, pp. 12-16, 2016.

[21] G. Liu, Y. Liu, and S. Gong, "Compact tri-band wide-slot monopole antenna with dual- ring resonator for WLAN/WiMAX applications," *Microwave & Optical Technology Letters*, vol. 58, no. 5, pp. 1097-1101, 2016.

[22] S. Imaculate Rosaline and S. Raghavan, "Meta-material inspired monopole antenna for WLAN/ WiMAX applications," *Microwave & Optical Technology Letters*, vol. 58, no. 4, pp. 936-939, 2016.

[23] R. S. Daniel, R. Pandeeswari, and S. Raghavan, "Design and analysis of metamaterial inspired open complementary split ring resonators for multiband operation," *Progress In Electromagnetics Research C*, vol. 78, pp. 173-182, 2017.

[24] A. S. M. Alqadami, M. F. Jamlos, J. S. Ping, S. K. A. Rahim, G. A. E. Vandenbosch, and A. Narbudowicz, "Miniaturized dual-band antenna array with double-negative (DNG) metamaterial for wireless applications," *Appl. Phys. A*, vol. 123, no. 1, p. 22, 2017.

[25] M. Alibakhshikenari, B. Virdee, A. Ali, and E. Limiti, "Miniaturized planar-patch antenna based on metamaterial L-shaped unit-cells for broadband portable microwave devices and multiband wireless communication systems," *IET Microwaves Antennas and Propagation*, vol. 12, no. 7, pp. 1080-1086, 2018.

[26] U. Patel and T. K. Upadhyaya, "Design and analysis of compact μ-negative material loaded wideband electrically compact antenna for WLAN/ WiMAX applications," *Progress In Electromagnetics Research*, vol. 79, pp. 11-22, 2019.